Journal of
Applied Crystallography
ISSN 0021-8898

Received 23 December 2000
Accepted 19 April 2001

Determination of γ' solution temperature in Re-rich Ni-base superalloy by small-angle neutron scattering

Pavel Strunz,[a,b]* Debashis Mukherji,[c] Ralph Gilles,[d] Albrecht Wiedenmann,[a] Joachim Rösler[c] and Hartmut Fuess[d]

[a]Hahn-Meitner Institut Berlin, Glienickerstr. 100, 14109 Berlin, Germany, [b]Nuclear Physics Institute, 25068 Řež near Prague, Czech Republic, [c]Technische Universität Braunschweig, Langer Kamp 8, 38106 Braunschweig, Germany, and [d]Technische Universität Darmstadt, Petersenstr. 23, 64287 Darmstadt, Germany. Correspondence e-mail: strunz@ujf.cas.cz

A harmful segregation of heavy elements (*e.g.* W, Mo, Re) during solidification of Ni-base superalloys can only be eliminated by using a homogenizing heat treatment, which needs to be carried out in the single-phase (γ) field above the γ' solvus temperature but below the solidus temperature. Small-angle neutron scattering (SANS) was employed for *in situ* observation of the dissolution of precipitates in an Re-rich superalloy. The temperature dependence of the relative volume fraction and the size distribution of smaller γ' precipitates, and the specific surface of large inhomogeneities as well as some other parameters were determined from the two-dimensional scattering curves measured for as-cast and heat-treated samples. Overlap of the incipient melting region with the region where a certain amount of precipitates remained undissolved was observed, thus complicating a determination of the temperature at which all γ' precipitates are already dissolved. Nevertheless, conclusions about the temperature at which the precipitates dissolve and about the temperature at which the incipient melting starts could be formulated. The total scattering probability is suggested as the measure of the overall homogeneity of the distribution of elements in the sample. The temperature dependence of this parameter indicates the optimum solution procedure.

1. Introduction

Ni-base superalloys are hardened by ordered γ' precipitates that are coherently embedded in the disordered γ-phase matrix. The γ' precipitate morphology, their volume fraction and their uniform distribution are important factors that determine the mechanical properties of the superalloy (Caron & Khan, 1983; MacKay & Nathal, 1990). Modern single-crystal alloys have very complex compositions and generally contain high amounts of heavy elements like W, Mo, Re, *etc*. They are generally cast alloys and segregation of heavy elements is common during solidification. The segregation has two harmful effects on the mechanical properties of the material. First, it leads to a non-uniform precipitate distribution. Second, it can cause the formation of undesirable secondary phases (TCP phases like σ, μ, *etc*.) in the interdendritic regions. The segregation of heavy elements during solidification can only be eliminated, at least partially, by using a homogenizing (solution) heat treatment, which has to be carried out in the single-phase (γ) region (see scheme in Fig. 1). Such a solution-treatment 'window' is thus defined by the solvus and the solidus temperatures. However, the solvus temperature (in modern superalloys above 1473 K) is very close to the melting temperature of the alloy in most commercial and experimental superalloys. For an optimum homogenization, the temperature must be high enough to cause dissolution of even the coarse interdendritic particles, but sufficiently low to avoid incipient melting. This window is very small in commercial alloys (ranging between 0 and ~30 K) and, in some cases, the incipient melting can even extend below the solvus temperature. A precise knowledge of the temperature range of this window is very important for optimization of the superalloy.

In the past, SANS was very useful in the characterization of bulk-averaged γ' morphology in single-crystal alloys. Our previous experiments (Strunz, Wiedenmann *et al.*, 1997; Gilles *et al.*, 1997; Strunz, Šaroun *et al.*, 1997; Gilles *et al.*, 1998; Strunz *et al.*, 1999; Mukherji *et al.*, 1999; Strunz, Zrník *et al.*, 2000) as well as literature data (Miller *et al.*, 1978; Bianchi *et al.*, 1988; Bellet, Royer *et al.*, 1992; Bellet, Bastie *et al.*, 1992; Paris *et al.*, 1993; Calderon *et al.*, 1994; Sequeira *et al.*, 1995; Aizawa *et al.*, 2000) show that γ' precipitates give rise to a strong SANS effect for many superalloys. Because of the low absorption of cold neutrons by the majority of elements, SANS can be used

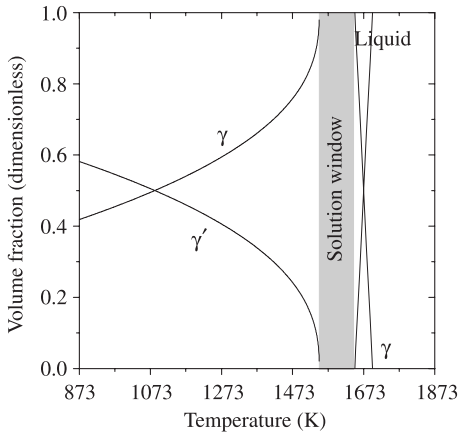

Figure 1
Schematic drawing of the solution window.

for *in situ* tests under extreme conditions (Miller *et al.*, 1978) and thus also for observation of dissolution of precipitates at high temperatures.

The small-angle scattering is caused by fluctuations of scattering length density $\rho(\mathbf{r})$ on a size scale of 20 Å–5 µm, connected with compositional and/or structural inhomogeneities (usually, but not exclusively, γ' precipitates in the case of superalloys). The fluctuations of scattering length density result in the scattering contrast $\Delta\rho(\mathbf{r}) = \rho(\mathbf{r}) - \bar{\rho}$ ($\mathbf{r}$ is the coordinate in real space; $\bar{\rho}$ is the average scattering length density of the sample). The scattering contrast gives rise to the coherent elastic scattering of neutrons to small magnitudes of the scattering vector ($Q = |\mathbf{Q}| = 4\pi\sin\theta/\lambda$, where $\mathbf{Q} = \mathbf{k} - \mathbf{k}_0$, $\mathbf{k}_0$ and $\mathbf{k}$ are the wavevectors of the incident and scattered neutrons, respectively, $|\mathbf{k}| = |\mathbf{k}_0| = 2\pi/\lambda$, 2θ is the full scattering angle, and λ is the incident neutron wavelength).

The aim of the *in situ* heating during SANS measurements as described herein was to take the two-phase superalloy into the single-phase γ region and to increase the temperature until incipient melting commenced. It is expected that the small islands of liquid phase formed as a result of the incipient melting can give rise to a strong contrast for neutrons and thus enable the detection of the upper limit of the solution-treatment window. This procedure should allow the determination of the solution window for the alloy and, at the same time, the evolution of the microstructure at high temperatures may be observed. Above 1373 K, such *in situ* observations are nearly impossible using other techniques. The *in situ* SANS measurements can improve the accuracy of determination of the solution window in bulk specimens and thereby improve the control of the heat-treatment parameters in cast single-crystal turbine blades for industrial application.

2. Experimental

Two samples (as-cast as well as heat-treated) of the Re-rich Ni superalloy designated Re13 (Ni–5.5Al–7.5Ta–7.0Re in wt%) were selected for the experiment. The details of the alloy composition are reported elsewhere (Mukherji & Rösler, 2001). The alloy has a large amount of heavy-element additions and therefore exhibits strong segregation.

Measurements were performed at the V4 facility (Keiderling & Wiedenmann, 1995; Berlin Neutron Scattering Centre, 2000*a*) in HMI Berlin, employing a standard ILL-type high-temperature furnace of BENSC (Berlin Neutron Scattering Centre, 2000*b*) equipped with a graphite-ceramics sample holder. The data were collected while the sample temperature was increased. The sample-to-detector distance was 16 m and λ was 19.4 Å. This geometry was selected in order to observe preferentially the solution of the largest γ' precipitates. Because of the low flux of the neutron source at such a wavelength, it was possible to make measurements without a beam-stop, which usually protects the two-dimensional position-sensitive detector (PSD) against overloading by non-scattered neutrons in the primary beam. The lower limit of the measured Q range is therefore restricted only by the resolution of the facility ($\Delta Q \simeq 0.0008$ Å^{-1}) for such a geometry.

Because of the uncertainty in the calibration of the furnace thermocouple and because of the temperature gradient between the thermocouple and the sample position (distance 2 cm), the furnace was calibrated by heating and melting small pieces of pure Ni. In this way, the temperature was determined within ± 5 K in the high-temperature region at the sample position.

The collection of SANS data was performed during pauses in the increase of temperature. The approximate holding time after each change of temperature was 30 min. The increase of temperature from one step to another was relatively fast (approximately 1 min).

The SANS analysis is complemented by electron microscopy. Fig. 2 displays the micrographs from both types of sample before the SANS experiment, as well as a micrograph indicating the incipient melting islands created during the *in situ* experiment. The information obtained from SANS experiments was combined with the thermal analysis and metallographic measurements of the heat-treatment window.

3. Results

The original material for both the as-cast and the heat-treated samples was polycrystalline with large grains. However, only one grain (or a set of grains having the maximum misorientation of 20°) was irradiated by neutrons in the investigated heat-treated sample during the experiment. This means that the scattering was anisotropic for this sample (for cuboidal precipitates oriented preferably with edges parallel to the ⟨100⟩ crystallographic directions, as is common after standard heat treatment of these superalloys). The term 'anisotropic' means an azimuthal dependence of the scattered intensity on the two-dimensional PSD. On the other hand, the scattering from the as-cast sample was isotropic; the term 'isotropic' means no azimuthal dependence and the whole scattering effect can be plotted as a one-dimensional dependence of the scattered intensity on Q.

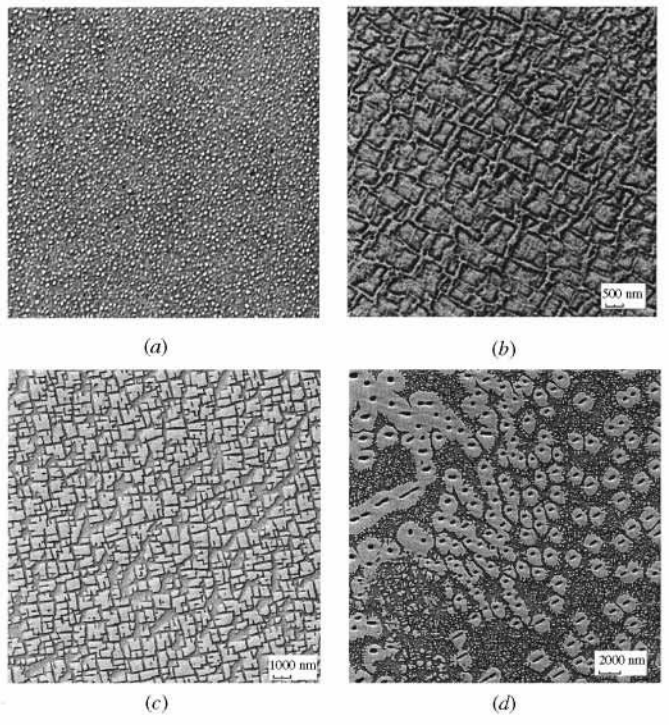

Figure 2
As-cast sample, initial condition: (*a*) γ' in dendrite region, (*b*) γ' in inter-dendrite region. Heat-treated sample: (*c*) initial condition, (*d*) example of incipient melting after heating to 1661 (5) K. In (*d*), the incipient melting island solidifies as γ' precipitates during cooling. The Re is rejected from this phase and forms Re-rich precipitates in the centre of these regions.

The necessary transmission measurement was performed for each temperature of each individual sample separately in order to avoid any influence of the diffuse scattering increase with temperature. The use of a special raw-data reduction procedure (Strunz, Šaroun *et al.*, 2000; Strunz, Wiedenmann *et al.*, 2000) allowed the transformation of measured intensities to cross sections even in the central part of the scattering curve where the scattering effect is combined with the rest of the non-scattered primary beam. In Fig. 3, the resulting SANS curves for the as-cast sample measured with increasing temperature are depicted. The lines through the points show the optimum fit of the microstructure model to the data for different temperatures. The applied model and the fit will be discussed below (§§4 and 5). Fig. 4 displays the two-dimensional scattering curves for the heat-treated sample measured with increasing temperature, together with the fitted model curves. Up to a certain temperature, the scattering is anisotropic as a result of the presence of cuboidal precipitates. The orientation of the precipitate edges with respect to the laboratory system (and thus also the orientation of the lattice of the grain) was found by fitting to be equal to $\omega = 47.9^\circ$, $\chi = 29.0^\circ$ and $\varphi = -30.5^\circ$. These rotations mean that the [100] direction is nearly parallel to the diagonal of the PSD and a strong intensity streak is thus observable in this direction. Around 1579 K, the already isotropic scattering indicates that nearly all cuboidal precipitates are dissolved. At the same

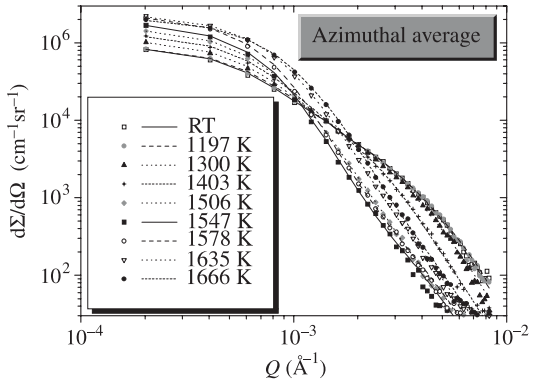

Figure 3
Measured (points) and fitted (lines) SANS curves of the as-cast Re-rich sample. The macroscopic differential cross section extracted from the azimuthally averaged two-dimensional data is plotted *versus* scattering vector magnitude.

time, the overall intensity of scattering is the lowest. When the temperature is further increased, the intensity of scattering again increases, but the isotropic character of the scattering data is retained.

4. Microstructure model

To treat the data in detail, the procedure suited for evaluation of anisotropic SANS (Strunz & Wiedenmann, 1997; Strunz, Wiedenmann *et al.*, 2000) was employed. The transformed model fitting method, which is the basis of the procedure, requires a model of microstructure to be input before the start of the fit.

The measured Q range allows for the determination of precipitate sizes between ~300 and ~5000 Å. For the as-cast sample, part of the precipitates (mainly in dendrites) have sizes within this range. They were thus directly modelled by their size distribution. The precipitates in the interdendritic region of the as-cast sample and in the whole heat-treated sample are larger (see Figs. 2*b* and 2*c*). In the original samples, the majority of precipitates have sizes between 4000 and 8000 Å. Their average size cannot be practically determined from SANS curves. The part of their size distribution up to 5000 Å precipitate size was thus approximated by particles of size equal to 4500 Å. The scattering curves are also sensitive to the γ' channel width between precipitates and to the width of the 'half-channels' penetrating some of the precipitates (see Fig. 2*c*). The average width of the channels is substantially smaller than the size of a precipitate itself. This width can thus be determined together with the relative volume fraction times the squared scattering contrast $(\Delta\rho)^2$ of this part of the size distribution (up to 5000 Å precipitate size) of the γ' precipitates.

At high temperatures, the smaller incipient melting islands (see Fig. 2*d*), or parts thereof of size 1500–5000 Å, can also give rise to the isotropic scattering and should be included in the model. The melted material (islands) can have a different scattering contrast from that of the solid before melting as a

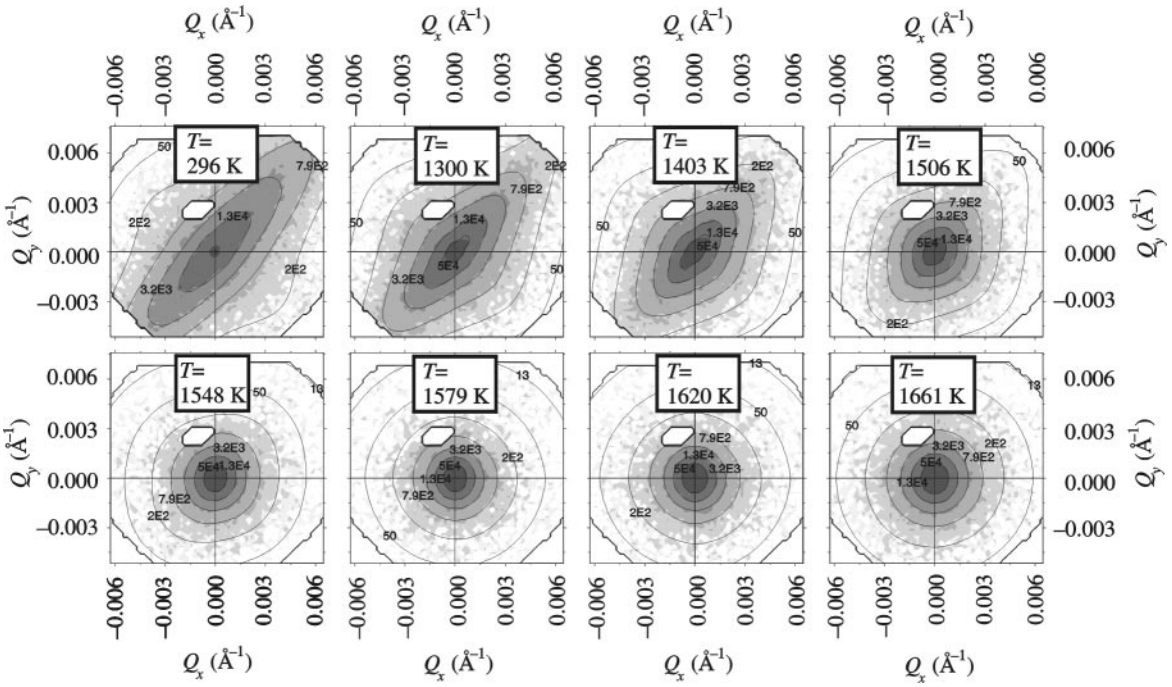

Figure 4
Selected measured (grey scale) and fitted (solid lines) two-dimensional scattering curves of the heat-treated sample. Displayed contour lines correspond to the equidistant levels of the macroscopic differential cross section $d\Sigma/d\Omega$ (cm^{-1} sr^{-1}) on a logarithmic intensity scale.

result of the difference of density and/or the loss of the internal structure of $\Delta\rho(\mathbf{r})$ within the incipient melting island.

A substantial amount of precipitates having sizes above 5000 Å exist in the samples. Incipient melting islands of size greater than 5000 Å can also be present above a certain temperature. All such inhomogeneities contribute to the scattered intensity, mainly in the central part of the scattering curve; however, the possibility to determine their size is substantially reduced because of the finite resolution of the facility. The only relevant parameter which can be deduced for such inhomogeneities is their specific surface multiplied by $(\Delta\rho)^2$. These inhomogeneities (large γ' precipitates and/or incipient melting islands) were modelled by large particles (15000 Å) having a certain specific surface during the evaluation.

To approximate the measured curves, the overall model was composed of several parts depending on the sample type and temperature. The individual parts are as follows.

(i) Small precipitates with sizes up to ∼3000 Å. These represent, in the majority, finer precipitates in the dendrites of the as-cast sample.

(ii) Larger precipitates (∼4500 Å) representing γ' phase in the interdendritic region (for the as-cast sample) or a part of the relatively homogeneously distributed precipitates in the heat-treated sample.

(iii) Fluctuations of scattering length density on the size scale 1500–5000 Å (smaller incipient melting islands).

(iv) Fluctuations of scattering length density with periods greater than 5000 Å (large precipitates and incipient melting islands).

For the as-cast sample, the model has to be, in principle, composed of all four parts. However, there is a transition when increasing the temperature during which the model (ii) is exchanged by the model (iii). The point (or rather temperature range) of transition from (ii) to (iii) cannot be precisely determined because of the isotropic character of scattering from both types of inhomogeneities. Therefore, scattering caused by model (ii) cannot be distinguished from scattering caused by (iii) and they can be treated together in the evaluation. Because of the non-zero scattering intensity in the whole measured Q range at all temperatures, the inhomogeneities described by both models (ii) and (iii) most probably overlap in a certain temperature range in the as-cast sample. The anisotropic scattering from the heat-treated sample allows one to separate better these two contributions: the anisotropic scattering has to be connected with the cuboidal precipitates and the temperature at which the precipitates disappear is thus better observable. However, the overlap cannot be excluded and a possible low scattering intensity from precipitates other than γ' has to be taken into account. In this (heat-treated) sample, the model (i) (small precipitates) is not used at all and the overall model is thus composed of two parts only [(ii) or (iii) plus (iv)].

As requested by the evaluation program (Strunz, Wiedenmann *et al.*, 2000), all the real-space models were input in the form of three-dimensional binary maps. Model (ii) had the distance between precipitates randomly smeared within the allowed range (no overlapping of neighbouring precipitates occurs). This approach introduces a distribution of the γ channel width.

5. Discussion

For the as-cast sample, the first dependencies determined from the fit are the temperature dependence of the size distributions of small particles in the dendrites (Fig. 5) and their relative volume fraction multiplied by $(\Delta\rho)^2$ (the inset in Fig. 5). It should be noted that the pure volume fraction cannot be determined because $\Delta\rho$ can slightly change with temperature. For Ni-base superalloys, the independent estimation of the average $\Delta\rho$ can usually only be made with a large uncertainty, even at room temperature (Gilles *et al.*, 1997); its precise determination at higher temperatures is then practically impossible.

It can be deduced that the small precipitates are completely dissolved above 1506 K and that their mean size increases from ~1200 Å to ~2000 Å in the temperature region 296–1506 K. This result means that the smaller precipitates dissolve or join other precipitate(s) to produce the coarse one(s) below 1506 K.

Fig. 6 displays the relative volume fraction (multiplied by square scattering contrast) for larger γ' precipitates (simulated by particles with size 4500 Å) both for the as-cast and the heat-treated sample. At 1579 K, the dependencies reach a minimum. The decrease of the volume fraction to zero cannot be observed at higher temperatures because of the fluctuations of scattering length density on a size scale of 1500–5000 Å [model (iii)]. Because of these inhomogeneities, further decrease of the scattering is not observed above 1579 K. The inhomogeneities can either be precipitates other than γ' which dissolve at still higher temperatures (in this case a nearly constant or slightly decreasing volume fraction is expected) or incipient melting islands (an increasing volume fraction as the temperature increases is expected). The volume fraction of these inhomogeneities is also displayed in Fig. 6 (high temperatures above 1579 K); the different scattering contrast compared with that of the precipitates has to be noted. For the as-cast sample, the majority of these inhomogeneities are the incipient melting islands (increasing volume fraction with temperature; see Fig. 6). The situation is less clear for the heat-treated sample: the increase of the curve in Fig. 6 is rather small and it can be assumed to be constant (within experimental error) up to 1635 K. Starting at this temperature, the formation of incipient melting islands (or their parts) of size up to 5000 Å is observed.

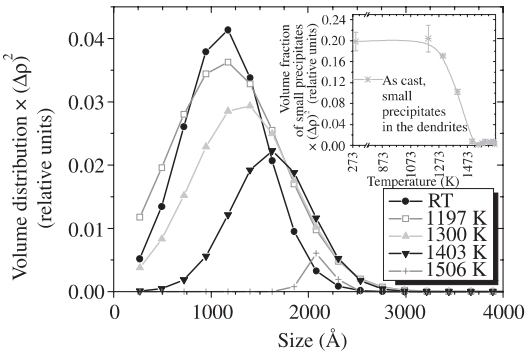

Figure 5
Distribution of particle volume with size for the smaller precipitates in dendrites. The inset displays the decrease of the volume of these precipitates with temperature.

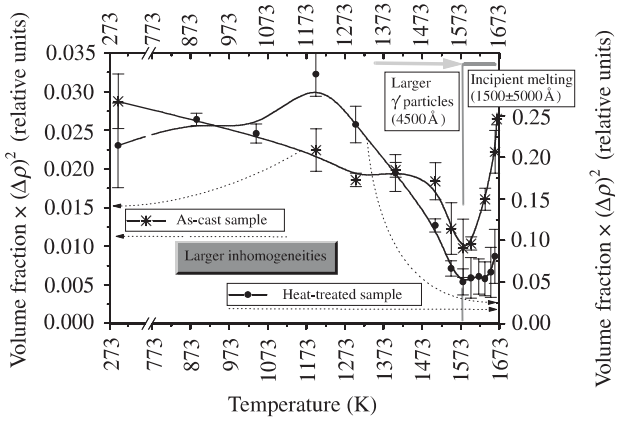

Figure 6
Volume fractions of precipitates of 4500 Å size for both as-cast and heat-treated samples. The lines through points are not fits; they are merely guides to the eye.

While the volume fraction multiplied by $(\Delta\rho)^2$ (Fig. 6) was determined basically from the absolute intensity of the scattering, another type of calculation can be performed if the geometrical parameters of the employed model are known. In Fig. 7, the selected real-space models corresponding to the fits of the larger γ' precipitates [model (ii)] to the heat-treated sample data are displayed up to the temperature at which they are observable. As can be seen, the γ channel width increases with temperature. If the determined width of the γ channel (see the inset of Fig. 8) is employed, the geometrical volume fraction of precipitates of 4500 Å size [model (ii)] can be calculated (Fig. 8). It confirms the decrease of volume fraction with temperature suggested by Fig. 6. The distortion by possibly changing scattering contrast is excluded here and the difference in shape of the curves in Figs. 6 (for the heat-treated sample) and 8 should be ascribed to a $\Delta\rho$ change with temperature.

The last point of the displayed dependence in Fig. 8 corresponds to the measurement at temperature 1548 K, at which the scattering was still anisotropic and thus the precipitates are still present. The following measurements at 1579 K and above show no anisotropy; this means that precipitates are dissolved or their volume fraction is non-measurable.

Scattering from large particles (scattering length density fluctuations), larger than 5000 Å, is represented by their specific surface multiplied by $(\Delta\rho)^2$ (Fig. 9). If we assume that their $\Delta\rho$ does not change substantially with temperature, the tendencies displayed in Fig. 9 are valid also for the specific surfaces. For the as-cast sample, the specific surface is approximately constant up to ~1503 K. Above 1548 K, the observed strong increase is caused by incipient melting.

For the heat-treated sample, the fitted specific surface is huge with respect to that of the as-cast sample at room temperature because there are many precipitates larger than

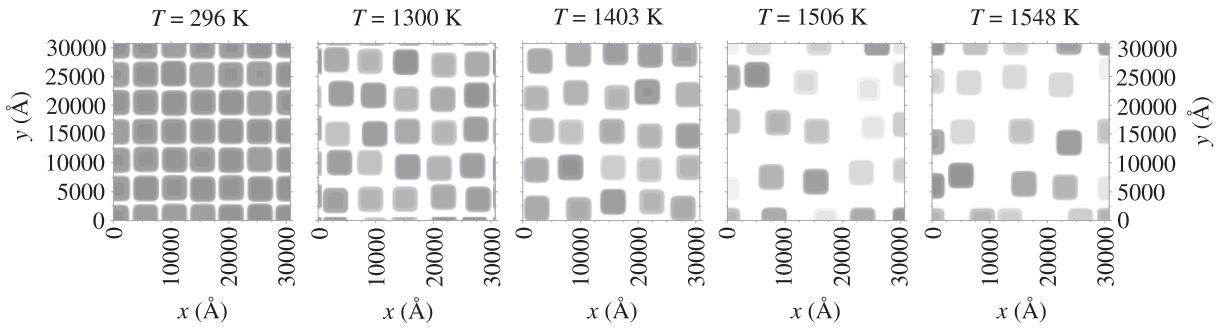

Figure 7
The real-space models of precipitates in the heat-treated sample corresponding to the fits in Fig. 4. The grey scale used to display the individual precipitate models comes from the method of imaging of the three-dimensional model to the two-dimensional graph: the central slice of the three-dimensional model with thickness equal to half the mean distance between particles was projected to two-dimensions assuming a certain transparency of the modelled precipitates.

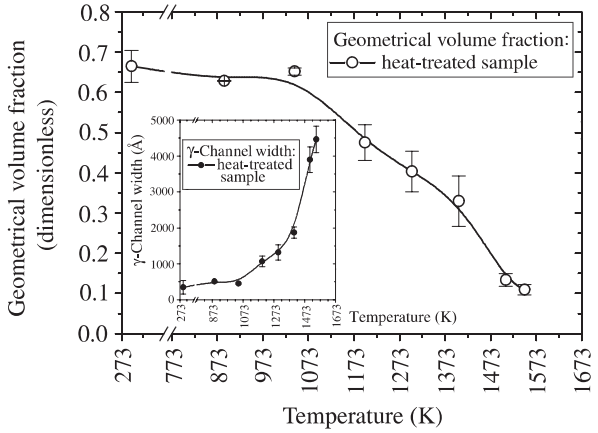

Figure 8
Results of the fit of the model: the geometrical volume fraction of precipitates of 4500 Å size and the width of the γ channel (inset) for the heat-treated sample.

5000 Å in the whole heat-treated sample, while such precipitates are present only in the interdendritic region in the as-cast sample. Their specific surface decreases up to approximately 1506 K. This effect is caused by joining the precipitates together. This process results in the growth of the precipitates but also in the decrease of their specific surface at the same time.

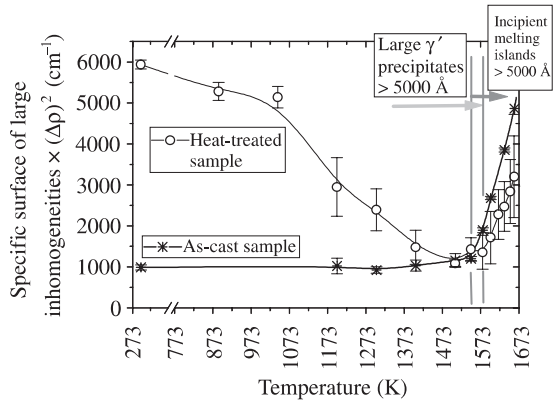

Figure 9
Specific surface of large inhomogeneities.

Above 1579 K, the strong increase can again be observed as a result of incipient melting. The start of the increase is shifted towards the higher temperatures with respect to the as-cast sample and the increase is not so steep. The same trend can be observed for small incipient melting islands (Fig. 6). The difference between the behaviour of the as-cast and heat-treated samples can be explained by larger compositional variations between the dendritic and interdendritic regions. There are, in fact, two alloys in the as-cast sample. These compositional variations implicate a broader incipient melting range for the as-cast alloy and thus the earlier onset of incipient melting.

Important information is also available from the total scattering probability (Schelten & Schmatz, 1980; Strunz, Šaroun *et al.*, 2000) obtained from the fit of the model. This probability is connected with the integral scattered intensity (Kostorz, 1979) and gives a measure of how homogeneously the elements are distributed in the sample. The evolution of the total scattering probability with temperature for our two samples can be observed in Fig. 10. The probability is the lowest at 1548 K for the as-cast sample, whereas the minimum is reached at 1579 K for the heat-treated sample. It has to be taken into account, however, that this measure is regardless of the size and the type of the inhomogeneity. This means that there can still be some non-dissolved precipitates in the minimums of the curves in Fig. 10; however, the incipient melting is still not strong and, altogether, the sample is the most homogeneous at this point.

6. Conclusions

The SANS data obtained in the presented experiment at various temperatures are a mixture of several contributions. Even though the applied model is relatively complex, it cannot cover all of the possible features of the material under study. Nevertheless, it reasonably describes the measured data and enables their interpretation; the fitted parameters thus contain useful information about the dissolution of precipitates, moreover obtained *in situ*.

The temperature dependence of the determined size distribution and volume fraction of small precipitates in the

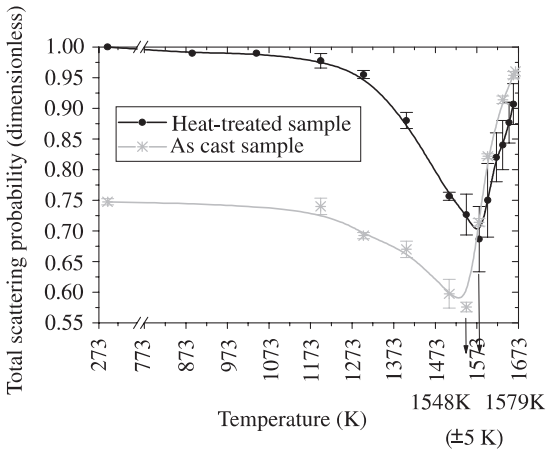

Figure 10
The total scattering probability *versus* temperature.

dendrites of the as-cast sample confirms that these particles dissolve deep below the necessary solution temperature. The volume of larger particles (in the interdendritic region of the as-cast sample and in the heat-treated sample) decreases, but less steeply, and they are present up to the region of the optimum solution treatment temperature, or even above it. The coalescence of particles larger than 5000 Å occurs in the heat-treated sample, resulting in the decrease of the specific surface with increasing temperature.

It was estimated that the incipient melting region overlaps with the temperature region where a certain amount of precipitates remain undissolved, at least for the as-cast sample. The incipient melting starts between 1548 K (large incipient melting islands detected above this temperature) and 1579 K [smaller (up to 5000 Å) incipient melting islands detectable above this temperature] for the as-cast sample, and between 1579 K (large islands above this temperature) and 1635 K (smaller islands detectable above this temperature) for the heat-treated one. To explain such a relatively broad temperature region where the incipient melting occurs (the melting temperature is 1676 K) in the as-cast sample, one has to take into account the compositional difference between the dendritic and interdendritic regions of the as-cast alloy as a result of strong segregation in this Re-bearing alloy. The incipient melting starts earlier in one of the regions than in the other. The presence of the temperature range where the incipient melting exists in the heat-treated sample indicates that the relatively large compositional fluctuations are also present after the heat treatment.

An interesting feature is that large (>5000 Å) incipient melting islands are 'visible' first; only after a certain increase of temperature does the scattering from the smaller ones (<5000 Å) appear. There are some possible mechanisms which could explain this effect. One probable explanation is that the small incipient melting islands are present prior to the large ones, but they are not detectable. While the incipient melting island had (because of the large diffusion in liquid) the constant scattering contrast in the whole melted region, the material had a certain spatial dependence of $\Delta\rho(\mathbf{r})$ in that region before the incipient melting island had been created. When the incipient melting island is small, the difference between $\Delta\rho(\mathbf{r})$ in the solid and the constant $\Delta\rho$ in the liquid is very small and a difference in scattering is visible only after a large number of incipient melting islands have been created. When the incipient melting island grows, this difference becomes larger (the scattering is thus detectable at lower temperatures) and, effectively, the inhomogeneity also becomes larger because the shorter-scale compositional fluctuations are removed inside the incipient melting island.

Because of the mixture of two contributions (precipitates–incipient melting islands), the point where all the precipitates are already dissolved can only be estimated (1579 ± 10 K). This estimation is more precise for the heat-treated sample because of the anisotropic character of scattering from cuboidal precipitates in the single grain.

From the point of view of the overall homogeneity of the distribution of elements in the sample, the total scattering probability is most likely the best measure of the temperature at which to perform the solution procedure. This point has been found to be different for the as-cast (1548 ± 10 K) and the heat-treated samples (1579 ± 10 K). The difference corresponds to the known fact that the optimum solution procedure should consist of at least two steps for this Re-rich superalloy in the as-cast form. The first step involves maintaining the lower temperature of ∼1548 K for a relatively long time; in the second step, an increase to ∼1583 K should be performed.

Two of the authors (RG and DM) thank BENSC for support enabling them to carry out the SANS experiment. The authors are indebted to Mr G. Steiner and Mr W. Graf (HMI Berlin) for technical assistance and to Professor M. Meissner (HMI Berlin), Dr A. Hoser (RWTH Aachen) and H. Schneider (TU München) for fruitful discussions.

References

Aizawa, K., Tomimitsu, H., Tamaki, H. & Yoshinari, A. (2000). *J. Appl. Cryst.* **33**, 847–850.
Bellet, D., Bastie, P., Royer, A., Lajzerowicz, J., Legrand, J. F. & Bonnet, R. (1992). *J. Phys. I (Paris)*, **2**, 1097–1112.
Bellet, D., Royer, A., Bastie, P., Lajzerowicz, J. & Legrand, J. F. (1992). *Superalloys 1992*, edited by S. D. Antolovich, R. W. Stusrud, R. A. MacKay, D. L. Anton, T. Khan, R. D. Kissinger & D. L. Klarstrom, pp. 547–556. Washington: The Minerals, Metals & Materials Society.
Berlin Neutron Scattering Centre (2000*a*). *V4 Small-Angle Neutron Scattering Instrument*, http://www.hmi.de/bensc/instrumentation/instrumente/v4/v4.html.
Berlin Neutron Scattering Centre (2000*b*). *U. S. E. Handbook*, http://www.hmi.de/bensc/sample-env/USE2000_4.pdf.
Bianchi, P., Carsughi, F., D'Angelo, D., Kulda, J., Mengoni, A., Mikula, P. & Rustichelli, F. (1988). *Mater. Sci. Forum*, **27–28**, 429–432.
Calderon, H. A., Voorhees, P. W., Murray, J. L. & Kostorz, G. (1994). *Acta Metall. Mater.* **42**, 991–1000.
Caron, P. & Khan, T. (1983). *J. Mater. Sci. Eng.* **61**, 173–184.
Gilles, R., Mukherji, D., Strunz, P., Wiedenmann, A. & Wahi, R. (1997). *Z. Metallkdd.* **88**, 518–521.

Gilles, R., Mukherji, D., Strunz, P., Wiedenmann, A. & Wahi, R. (1998). *Physica B*, **241–243**, 347–349.
Keiderling, U. & Wiedenmann, A. (1995). *Physica B*, **213–214**, 895–897.
Kostorz, G. (1979). *Neutron Scattering* (*Treatise on Materials Science and Technology*), edited by G. Kostorz, pp. 227–289. New York: Academic Press.
MacKay, R. A. & Nathal, M. V. (1990). *Acta Metall. Mater.* **38**, 993–1005.
Miller, R. J. R., Messoloras, S., Stewart, R. J. & Kostorz, G. (1978). *J. Appl. Cryst.* **11**, 583.
Mukherji, D., Gilles, R., Strunz, P., Lieske, S., Wiedenmann, A. & Wahi, R. (1999). *Scr. Mater.* **41**, 31–38.
Mukherji, D. & Rösler, J. (2001). *J. Mater. Proc. Technol.* Submitted (Proceedings of Thermec 2000, Las Vegas, 4–8 December 2001).
Paris, O., Fährmann, M. & Fratzl, P. (1993). *Phys. Rev. Lett.* **75**, 3458–3461.
Schelten, J. & Schmatz, W. (1980). *J. Appl. Cryst.* **13**, 385–390.
Sequeira, A. D., Calderon, H. A., Kostorz, G. & Pedersen, J. S. (1995). *Acta Metall. Mater.* **43**, 3427–3439.
Strunz, P., Gilles, R., Mukherji, D., Wiedenmann, A., Wahi, R. & Zrník, J. (1999). *Mater. Struct.* **6**, 1–5. (Proceedings of 18th European Crystallographic Meeting, August 15–20, 1998, Prague, Czech Republic.)
Strunz, P., Šaroun, J., Keiderling, U., Wiedenmann, A. & Przenioslo, R. (2000). *J. Appl. Cryst.* **33**, 829–833.
Strunz, P., Šaroun, J., Mikula, P., Lukáš, P. & Eichhorn, F. (1997). *J. Appl. Cryst.* **30**, 844–848.
Strunz, P. & Wiedenmann, A. (1997). *J. Appl. Cryst.* **30**, 1132–1139.
Strunz, P., Wiedenmann, A., Gilles, R., Mukherji, D., Zrník, J. & Schumacher, G. (2000). *J. Appl. Cryst.* **33**, 834–838.
Strunz, P., Wiedenmann, A., Zrník, J. & Lukáš, P. (1997). *J. Appl. Cryst.* **30**, 597–601.
Strunz, P., Zrník, J., Gilles, R. & Wiedenmann, A. (2000). *Physica B*, **276–278**, 890–891.